Available online at www.sciencedirect.com
ScienceDirect
Ceramics International 37 (2011) 3413–3417
CERAMICS INTERNATIONAL
www.elsevier.com/locate/ceramint

Sol–gel derived $6CaO{\cdot}6SrO{\cdot}7Al_2O_3$ thin films using metal alkoxides

P.M. Chavhan [a,b,c,*], Anubha Sharma [b], R.K. Sharma [a,*], CheolGi Kim [c], N.K. Kaushik [b]

[a] Polymeric and Soft Material Section, National Physical Laboratory, Dr. K.S. Krishnan Road, New Delhi 110012, India
[b] Department of Chemistry, University of Delhi, Delhi 110007, India
[c] Department of Materials Science and Engineering, Chungnam National University, Daejeon-305764, Republic of Korea

Received 25 April 2011; received in revised form 31 May 2011; accepted 31 May 2011
Available online 12 June 2011

Abstract

The novel $6CaO{\cdot}6SrO{\cdot}7Al_2O_3$ (C6S6A7) thin films were deposited onto soda lime glass substrate using calcium, strontium, aluminium isopropoxide and 2-methoxy ethanol as starting materials via sol–gel dip coating technique. The electrical and optical properties of C6S6A7 films were investigated for films sample annealed at 450 °C for 2 h in air and hydrogen (H_2) atmosphere, respectively. X-ray diffraction pattern and Fourier transformed infrared spectroscopy analysis confirms cubic structure to the C6S6A7 material. The optical transmission spectra of C6S6A7 films showed the high transparency in wide visible range of ~ 88 and 80% for air and H_2 annealed samples, respectively. The C6S6A7 films sheet resistance of 528 and 0.65 k Ohm/square has been observed for films annealed in air and H_2 atmosphere at 450 °C, respectively.

Keywords: C. Optical properties; Sol–gel; 2-Methoxy ethanol; C6S6A7 films; Sheet resistance

1. Introduction

Alkaline earth metal oxides combined with aluminium oxide have potential use as refractory oxides in the steel industry and binder materials in the cement industry. They are of great interest in materials science because of their use as long-duration photoluminescence and thermo luminescence pigments [1]. In the $CaO–Al_2O_3$ binary system, $CaO{\cdot}Al_2O_3$ (CA), $CaO{\cdot}2Al_2O_3$ (CA2), $12CaO{\cdot}7Al_2O_3$ (C12A7) are the extensively studied oxide which has been exploited during aluminous cement production [2]. There have been numerous reports on C12A7 thin films deposited by pulsed laser deposition (PLD) technique [3–5]. The C12A7 is a promising binary compound with potential uses in electronic and optoelectronic devices [6]. However, it suffers from some drawbacks such as necessity to prepare target material prior to deposition, the chance of particulates deposition and the lack of uniformity over large areas [7,8]. Compared with the better known $CaO–Al_2O_3$ system, the $SrO–Al_2O_3$ system [9] has also the existence of SA, SA2 and S12A7 stable double oxides, isostructural with CA, CA2 and C12A7 (in the cement chemistry notation C = CaO, S = SrO and A = Al_2O_3). S12A7 is a meta-stabilized phase in the $SrO–Al_2O_3$ system and has the same structure as C12A7 system. S12A7 has larger lattice parameters as compared to C12A7 and, which is converted in to stable electride thin films [10]. The synthesis of bulk S12A7 was first carried out by a sol–gel process [11]. The nanostructured pulsed laser deposited (PLD) C12A7 thin film is a promising binary compound with potential uses in electronic and optoelectronic devices [6] and its nanoporous crystal structure is responsible for the oxygen ion generation, H^- ion emission and electron emission at room temperature [12–15]. However, PLD C12A7 thin films require the preparation of target material prior to deposition and the lack of uniformity over large areas [16]. Moreover in the preparation of multicomponent mixed oxide thin films, the sol–gel process represents an attractive alternative to conventional synthesis methods. Compared to solid state reactions, this mild synthesis method usually results in the formation of mixed oxide of improved homogeneity [17–19].

In present work, we synthesized C6S6A7 thin films using sol–gel dip coating technique wherein six Ca^{2+} ions has been substituted by six Sr^{2+} ions in the cage like C12A7 structure. The C6S6A7 thin films have been characterized by XRD, FT-IR and UV–visible spectroscopy. The optical transparency and sheet resistance of films has been evaluated using UV–visible

* Corresponding authors. Tel.: +91 11 25742610; fax: +91 11 25742612.
E-mail addresses: pandurang.chavhan@gmail.com (P.M. Chavhan), rksharmanpl@rediffmail.com (R.K. Sharma), cgkim@cnu.ac.kr (C.G. Kim).

0272-8842/$36.00
doi:10.1016/j.ceramint.2011.05.144

spectra and four point probe method. Jestin et al. have reported low-loss optical Er^{3+}activated glass-ceramics planar waveguides fabricated by bottom-up approach. The dip coating technique is very useful for fabrication of sol–gel derived integrated optics systems [20]. The sol–gel process is regarded as being a cost-effective and simple technique which can easily lead to the formation of uniform thin films at room temperature offering precise control over the stoichiometry of the deposited film [21].

2. Experimental details

2.1. Materials and solvents

Calcium (Ca) and Strontium (Sr) metal pieces with more than 99% purity were purchased from Sigma–Aldrich Chemie, Germany. Aluminium isopropoxide with more than 99% in purity was purchased from Riedel de Haen, Seelze and 2-methoxy ethanol with more than 99.5% purity was purchased from LOBA Chemie, Pvt. Ltd., Mumbai.

2.2. Preparation of sol

C6S6A7 sol was prepared using stoichiometric amount of Ca-2-ethyl hexonate, Sr-glyconate monomethyl ether and aluminium isopropoxide as precursor materials. Ca-2-ethyl hexonate were prepared by refluxing calcium metal with 2-ethyl hexonic acid using 2-methoxy ethanol as a solvent. Similarly, Sr-glyconate monomethyl ether was prepared by refluxing strontium metal in 2-methoxy ethanol.

As prepared Ca-2-ethyl hexonate and Sr-glyconate monomethyl ether were mixed well by shaking for 10 min to prepare homogenous sol. In this sol an adequate amount of aluminium iso-propoxide was added drop wise with continuous stirring. The solution was diluted to 100 ml by using 2-methoxy ethanol in order to prepare 2% sol [22]. The prepared precursor sol was stirred for 0.5 h and kept 2 h for aging. A schematic representation of sol preparation steps is shown in Fig. 1.

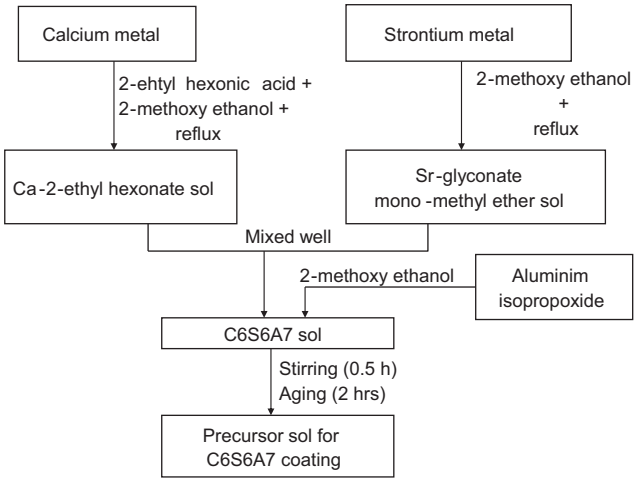

Fig. 1. Schematic representation of precursor sol for C6S6A7 coatings.

2.3. Deposition of C6S6A7 thin films

Soda lime float glass plates (2.5 cm × 7.5 cm) were used for coating of C6S6A7 thin films. Glass plates initially cleaned with distilled water were washed with 10% NaOH (caustic solution) followed by cleaning with distilled water. Again substrate plates were dipped in chromic acid for 5 min to remove associated organic impurities and finally after acid treatment plates were washed with plenty of distilled water and dried in an oven at 120 °C. Prior to coating, glass substrates were again cleaned with acetone and visually checked for dust or any other particles.

Thin films of C6S6A7 were coated onto soda lime float glass substrate using 15 cm/min lifting speed and 2% sol using sol–gel dip coating technique. Desired films thickness has been controlled by multiple coatings. After each coating, they were dried at 100 °C for 10 min. A thickness of about 65 nm of a single layer was obtained. The coating process was repeated 2 and 3 times to synthesize C6S6A7 films of higher thicknesses. Finally all samples were annealed at 450 °C for 2 h in air and H_2 atmosphere, respectively.

2.4. Characterizations

Thickness of the films was measured by using FILMETRICS-F20 thin film analyzer. X-ray diffraction (XRD) was used for crystal phase identification. XRD measurements were carried out on a Bruker AXS D8 Advance diffractometer using Diffrac^{plus} software. Diffractograms were recorded in grazing incidence geometry using CuKα radiation. The FT-IR spectra of C6S6A7 films were recorded using Perkin–Elmer Model BX2 spectrophotometer in the wave number range of 400–4000 cm^{-1}. Optical transmission spectra were recorded in the 200–800 nm range using SHIMADZU UV-3101 spectrophotometer at normal incidence. Films sheet resistance was recorded using four probe point measurement method.

3. Results and discussion

3.1. X-ray diffraction analysis

Fig. 2 shows the XRD patterns of C6S6A7 thin films annealed at 450 °C in air atmosphere. The prominent peaks resolved by X-ray diffraction analysis are observed at 20.1, 25.5, 31.8, 36.7, 41.8, 46.9, 54.1, 58.1 diffraction angle which are assigned to 211, 400, 420, 422, 521, 611, 640, 642 lattice planes confirms the cubic phase. However, peaks resolved at 29.9, 44.7 and 50.6 in the diffraction pattern indicate existence of unknown phase in the C6S6A7 material. The appearance of low intensity peaks with unknown phase in the XRD pattern may give deformed cubic structure to the C6S6A7 material. The formation of deformed crystal structure may be because of substitution of six Ca^{2+} ions by six Sr^{2+} ions in the cage like unit cell of C12A7 in the C6S6A7 material. According to Scherrer formula [$D = 0.9\lambda/\beta \cos\theta$] [23], the particle size of the annealed sample has been calculated to be approximately 6 nm.

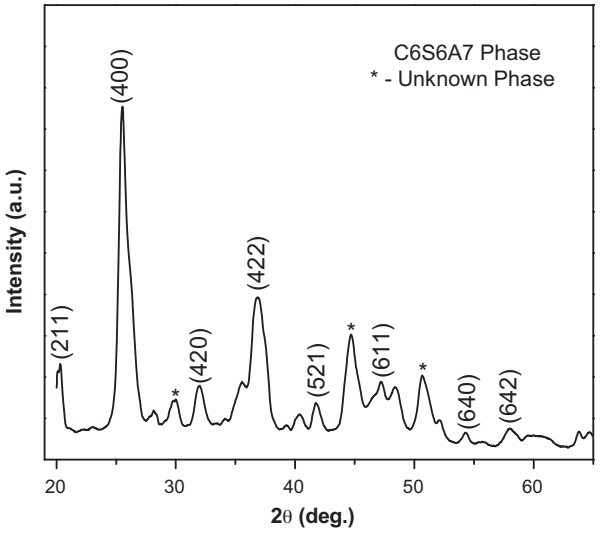

Fig. 2. XRD patterns of C6S6A7 thin films annealed at 450 °C in air atmosphere.

3.2. Fourier transformed infrared spectroscopic analysis

The FT-IR spectra of C6S6A7 thin films annealed at 450 °C in air and H_2 atmosphere is shown in Fig. 3. The most prominent peaks are observed nearly 3545 and 1269 cm^{-1} due to the presence of absorbed moisture and CO_3^- from organometallic precursor or organic solvents traces incorporated during film deposition, respectively [22]. The typical broad strong IR absorption ~815 cm^{-1} is attributed to the stretching vibrations of Ca–O and Sr–O bonding and stretching vibration peak ~558 cm^{-1} attributed to Al–O bonding. Moreover, absorption peaks in the 550–850 cm^{-1} region are attributed to the characteristic absorption corresponding to the Al–O stretching and bending modes in AlO_4 tetrahedral [24,25]. There is a distinguishable and repeatable peak near 3545 cm^{-1}; which assigned to the stretching vibration of O–H on the films surface due moisture present on the films [26–28].

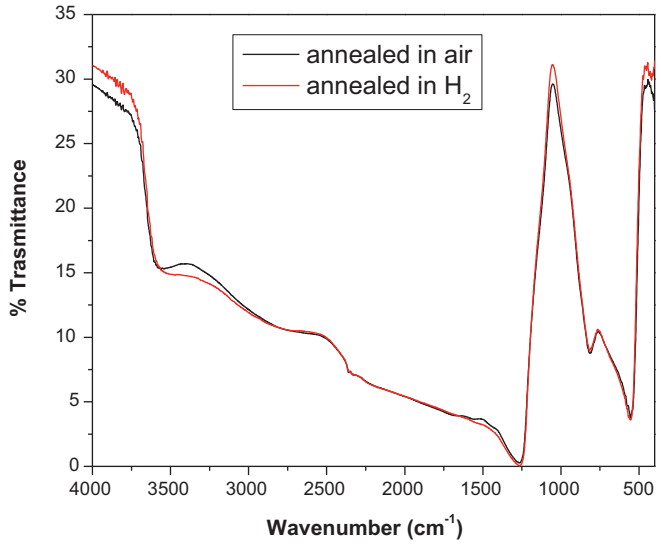

Fig. 3. FT-IR spectrum of C6S6A7 thin films using 2% sol concentrations and annealed at 450 °C.

3.3. Optical properties

Fig. 4a shows the UV–visible transmission pattern of C6S6A7 thin films (129 nm) deposited onto glass substrate and annealed at 450 °C for 2 h in air and H_2 atmosphere. The transmission data of C6S6A7 films annealed in air and H_2 was recorded by dividing transmission of the films to transmission of soda lime glass in all samples. The C6S6A7 films deposited using 2% sol on glass substrate and annealed at in air and H_2 atmosphere showed an average transparency of ~88% and 80% in wide visible range, respectively. The optical transparency is much lower mainly due to electron transitions between the valence and conduction band. In the UV region, the optical transmittance falls sharply, indicating the onset of absorption in this region. The threshold of optical absorption for C6S6A7 films annealed in H_2 atmosphere shifts toward shorter wavelengths, suggesting a broadening of the optical band gap. The observed optical interferences in the transmittance curve indicate a homogenous nature of the film.

In order to calculate the band gap energy (E_{opt}) of the C6S6A7 thin films, we assume the absorption coefficient $\alpha = (1/d)\ln(1/T)$, where T is transmittance and d is the thickness. Fig. 4b shows the graph of $(\alpha h\nu)^2$ Vs. photon energy ($h\nu$) of C6S6A7 films (129 nm) annealed in air and H_2 atmosphere,

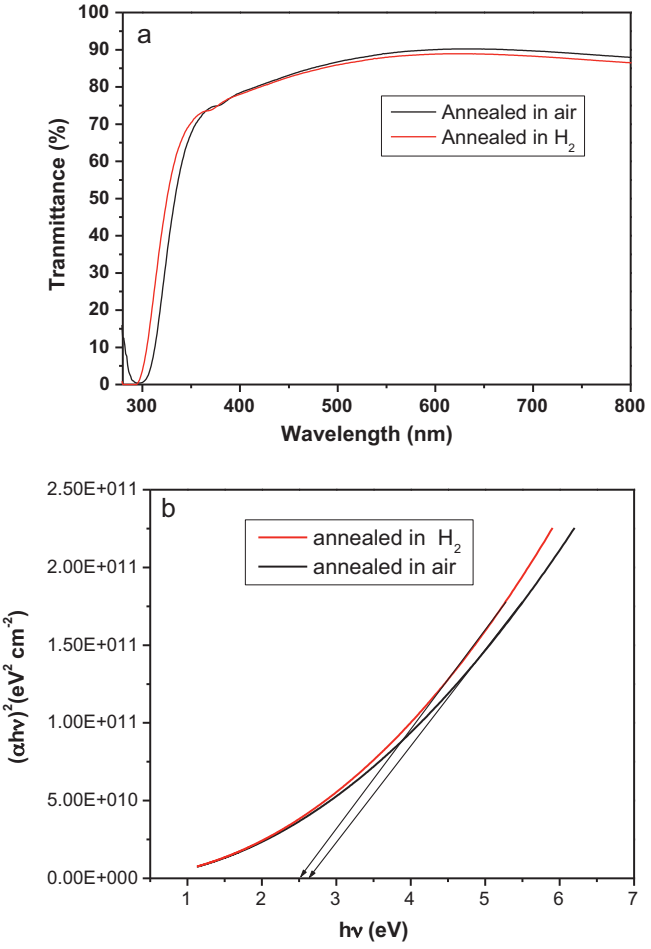

Fig. 4. (a) UV–vis transmission spectra; (b) Plot of $(\alpha h\nu)^2$ Vs. photon energy $h\nu$ of C6S6A7 thin films (129 nm) annealed in air and H_2 at 450 °C for 2 h.

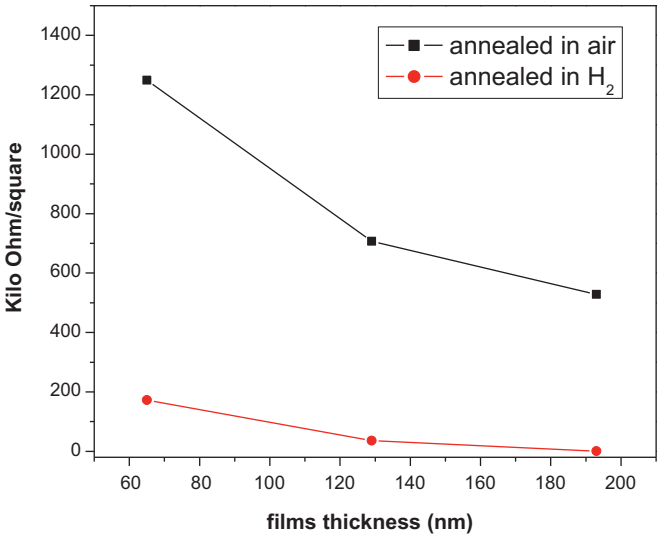

Fig. 5. Variation in sheet resistance values as a function of film thickness for C6S6A7 films annealed at 450 °C in air and H_2 for 2 h.

respectively. The linear dependence of $(\alpha h\nu)^2$ on $h\nu$ at higher photon energies indicate that the C6S6A7 films are essentially direct-transition-type semiconductors. The straight portion of the curve, when extrapolated to zero, gives the optical band gap E_{opt}. The E_{opt} of the C6S6A7 thin films evaluated (Fig. 4b) is nearly 2.51 eV and 2.63 eV for air and H_2 annealed films, respectively.

3.4. Electrical properties

The electrical properties of C6S6A7 thin films derived by sol–gel process have been investigated after thermal treatment in air and H_2 atmosphere. The sheet resistance measurements of C6S6A7 thin films were carried out by taking five readings for each thickness and the mean values are plotted. The error was between ±2%. The sheet resistance values have been found to be decreased with increase in the coatings thickness in both air and H_2 annealed C6S6A7 samples. The decrease in sheet resistance with increase coating thickness may be attributed to increase in carrier concentration which gives larger mean free paths and further leads to relatively high carrier mobility. This may be due to fact that at lower thickness films consists of anion trap centers, which may be possibly responsible for high sheet resistance.

The changes in sheet resistance values with changes in coating thickness of C6S6A7 films for samples annealed in air and H_2 atmosphere are shown in Fig. 5. The sheet resistance of C6S6A7 films of 193 nm observed to be 528 and 0.65 k Ohm/square for air and H_2 annealed samples, respectively. The resistance values significantly decreased after annealing in H_2 atmosphere. The significant decreases in sheet resistance values of H_2 annealed films could be attributed to the increase in oxygen vacancies resulting in increase in the carrier concentration and lowering the overall resistivity. This may be ascribed to the larger mean free path which leads to relatively high carrier mobility and thereby lowering the sheet resistance to 0.65 k Ohm/square for C6S6A7 films of nearly same thickness. It may be mentioned that sheet resistance was measured within a week of sample preparation. However, it has been observed that after one month of deposition the sheet resistance values increased nearly 3% of the values recorded within a week.

4. Conclusions

In the present work, the transparent conducting C6S6A7 thin films have been coated onto soda lime float glass substrate by sol–gel dip coating technique based on hydrolysis, condensation and polycondensation reactions using metal alkoxides. The XRD and FT-IR analyses confirmed that the C6S6A7 films annealed in air/H_2 atmosphere have cubic phase structure. The C6S6A7 films showed an average transparency of ∼88% and 80% in wide visible range for air and H_2 annealed samples, respectively. The E_{opt} of the C6S6A7 films has been observed to be enhanced when films has been annealed in H_2 atmosphere. The C6S6A7 films exibited sheet resistance of 528 and 0.65 k Ohms/square for air and H_2 annealed samples, respectively.

Acknowledgements

The authors would like to thank to Dr. Vinod for recording XRD data of the samples. The author gratefully acknowledges the help rendered by Mr. Ajeet Kaushik in obtaining FT-IR patterns. This research was partly supported by BK21 and WCU (R32-20026) are sincerely acknowledged. We are also thankful to Director, National Physical Laboratory for providing the facilities.

References

[1] F.C. Pallila, A.K. Levine, M.R. Tomkus, Fluorescent properties of the alkaline earth aluminates of the type MAl_2O_3 activated by divalent europium, Journal of Electrochemical Society 115 (1968) 642–644.
[2] K.S. Fukuda, I.H. Yoshida, Cationic substitution in tricalcium aluminate, Cement and Concrete Research 33 (2003) 1771–1775.
[3] M. Miyakawa, Y. Toda, K. Hayashi, M. Hirano, T. Kamiya, N. Matsunami, H. Hosono, Formation of inorganic electride thin films via site-selective extrusion by energetic inert gas ions, Journal of Applied Physics 97 (2005) 0235101–0235106.
[4] Y. Toda, M. Miyakawa, K. Hayashi, T. Kamiya, M. Hirano, H. Hosono, Thin film fabrication of nano-porous $12CaO{\cdot}7Al_2O_3$ crystal and its conversion into transparent conductive films by light illumination, Thin Solid Films 445 (2003) 309–312.
[5] M. Miyakawa, M. Hirano, T. Kamiya, H. Hosono, High electron doping to a wide band gap semiconductor $12CaO{\cdot}7Al_2O_3$ thin film, Applied Physics Letter 90 (2007) 182105–182107.
[6] T. Kamiya, H. Hosono, Creation of new functions in transparent oxides utilizing nanostructures embedded in crystal and artificially encoded by laser pulses, Semiconductor Science and Technology 20 (2005) S92–S102.
[7] J. Gottman, E.W. Kreutz, Pulsed laser deposition of alumina and zirconia thin films on polymers and glass as optical and protective coatings, Surface Coating and Technology 116–119 (1999) 1189–2294.
[8] Q. Bao, C. Chen, D. Wang, Q. Ji, T. Lei, Pulsed laser deposition and its current research status in preparing hydroxyl apatite thin films, Applied Surface Science 252 (2005) 1538–1544.
[9] F. Massazza, The system $SrO–Al_2O_3$, Chimistry & Industry (Milan) 41 (1959) 108–115.
[10] M. Miyakawa, N. Ueda, T. Kamiya, M. Hirano, H. Hosono, Novel room temperature stable electride $12SrO{\cdot}7Al_2O_3$ thin films: fabrication, optical

and electron transport properties, Journal of Ceramic Society of Japan 115 (9) (2007) 567–570.
[11] O. Yamaguchi, A. Narai, K. Shimizu, New compound in the system $SrO{\cdot}Al_2O_3$, Journal of American Ceramic Society 69 (2) (1986) C36–C37.
[12] Q. Li, K. Hayashi, M. Nishioka, H. Kashiwagi, M. Hirano, Y. Torimoto, H. Hosono, M. Sadakata, Absolute emission current density of O^- from $12CaO{\cdot}7Al_2O_3$ crystal, Applied Physics Letter 80 (2002) 4259–4261.
[13] T. Kamiya, S. Aiba, M. Miyakawa, K. Nomura, S. Matsuishi, K. Hayashi, K. Ueda, M. Hirano, H. Hosono, Field-induced current modulation in nanoporous semiconductor electron-doped $12CaO{\cdot}7Al_2O_3$, Chemistry of Material 17 (2005) 6311–6316.
[14] Q. Li, H. Hosono, M. Hirano, K. Hayashi, M. Nishioka, H. Kashiwagi, Y. Torimoto, M. Sadakata, High-intensity atomic oxygen radical anion emission mechanism from $12CaO{\cdot}7Al_2O_3$ crystal surface, Surface Science 527 (1–3) (2003) 100–112.
[15] H. Hosono, Functioning of traditional ceramics $12CaO{\cdot}7Al_2O_3$ utilizing built-in nano-porous structure, Science and Technology of Advanced Materials 5 (2004) 409–416.
[16] J. Gottmann, E.W. Kreutz, Pulsed laser deposition of alumina and zirconia thin films on polymers and glass as optical and protective coatings, Surface Coating and Technology 116–119 (1999) 1189–1194.
[17] J.M. Thomas, Design, synthesis, and in situ characterization of new solid catalysts, Angewandte Chemie International Edition 38 (24) (1999) 3588–3628.
[18] R.C. Mehrotra, Precursors for aerogels, Journal of Non-Crystalline Solids 145 (1992) 1–10.
[19] H. Schimidt, Chemistry of material preparation by the sol–gel process, Journal of Non-Crystalline Solids 100 (1998) 51–64.
[20] Y. Jestin, C. Armellini, A. Chiasera, A. Chiappini, M. Ferrari, E. Moser, R. Retoux, G.C. Righini, Low-loss optical Er^{3+}-activated glass-ceramics planar waveguides fabricated by bottom-up approach, Applied Physics Letters 91 (2007), pp. 071909-1/3.
[21] A.C. Pierre, Introduction to Sol–Gel Processing, Kluwer, Boston, MA, 1998, p. 2.
[22] P.M. Chavhan, A. Sharma, R.K. Sharma, Govind, C.G. Kim, N.K. Kaushik, Structural and optical properties of $6CaO{\cdot}6SrO{\cdot}7Al_2O_3$ thin films derived by sol–gel dip coating process, Journal of Non-Crystalline Solids 357 (2011) 1351–1356.
[23] B.D. Cullity, Elements of X-Ray Diffraction, Adison-Wesley, London, 1959, p. 261.
[24] C.F. Windisch, K.F. Ferris, G.J. Exarhos, Synthesis and characterization of transparent conducting oxide cobalt–nickel spinel films, Journal of Vacuum Science and Technology A-Vacuum Surface and Films 19 (4) (2001) 1647–1651.
[25] C.F. Windisch, K.F. Ferris, G.J. Exarhos, S.K. Sharma, Conducting spinel oxide films with infrared transparency, Thin Solid Films 420 (2002) 89–99.
[26] P. Tarte, Infra-red spectra of inorganic aluminates and characteristic vibrational frequencies of AlO_4 tetrahedra and AlO_6 octahedra, Spectrochimica Acta A 23 (1967) 2127–2143.
[27] R.A. Schroeder, L.L. Lyons, Infra-red spectra of the crystalline inorganic aluminates, Journal of Inorganic and Nuclear Chemistry 28 (1966) 1155–1163.
[28] T. Tashiro, T. Watanabe, M. Kawasaki, K. Toi, T. Ito, Partial oxidation of methane with oxygen over magnesium oxide at low temperatures, Journal of Chemical Society 89 (1993) 1263–1269.